Thermo-mechanical modelling of a superelastic shape-memory wire under cyclic stretching–bending loadings

Ferdinando Auricchio [a,*], Elio Sacco [b]

[a] *Dipartimento di Meccanica Strutturale, Università di Pavia, Via Ferrata 1, 27100 Pavia, Italy*
[b] *Dipartimento di Meccanica, Strutture, A&T, Università di Cassino, Via Di Biasio 43, 03043 Cassino, Italy*

Abstract

Experimental investigations on superelastic shape-memory alloy wires show a significant dependency of the load–displacement response on the loading–unloading rate, coupled with a non-negligible oscillation of the wire temperature.

Motivated by this observation, the present work proposes a thermo-mechanical model, suitable to study the response of a superelastic shape-memory alloy wire under cyclic stretching–bending loadings.

The model is based on the kinematical assumptions that sections which are plane in the undeformed configuration remain plane also in the deformed configuration and that the wire shear deformation is negligible. As a consequence, we need to introduce only a one-dimensional constitutive stress–strain equation; this relation involves a scalar internal variable, representing the martensite fraction, variable for which evolutionary equations are proposed.

The whole model is then thermo-mechanically coupled due to the presence of internal heat sources in the form of phase-transition latent heat and of mechanical dissipation.

The paper also addresses a numerical scheme for the integration, in time, of the model and the algorithmic solution of the corresponding time-discrete thermo-mechanical problem. Finally, results from numerical simulations are presented to show the response of a wire under cyclic stretching and bending loading conditions imposed at different strain-rates. © 2001 Elsevier Science Ltd. All rights reserved.

Keywords: Stretching–bending loadings; Superelastic; Thermo-mechanical modelling

1. Introduction

A large class of materials, known as *shape-memory alloys* (SMAs), presents the *superelastic effect*, that is, the ability of undergoing large deformations in loading–unloading cycles without showing residual deformations at the end of the cycles (Buehler and Wiley, 1965; Wayman and Duerig, 1990; Wayman, 1992, 1993). As an example, Fig. 1 reports a typical superelastic response in tension and compression extracted from Lim and McDowell (1999).

---

[*] Corresponding author. Tel.: +39-0382-505-476; fax: +39-0382-528-422.
E-mail addresses: auricchio@unipv.it (F. Auricchio), sacco@ing.unicas.it (E. Sacco).
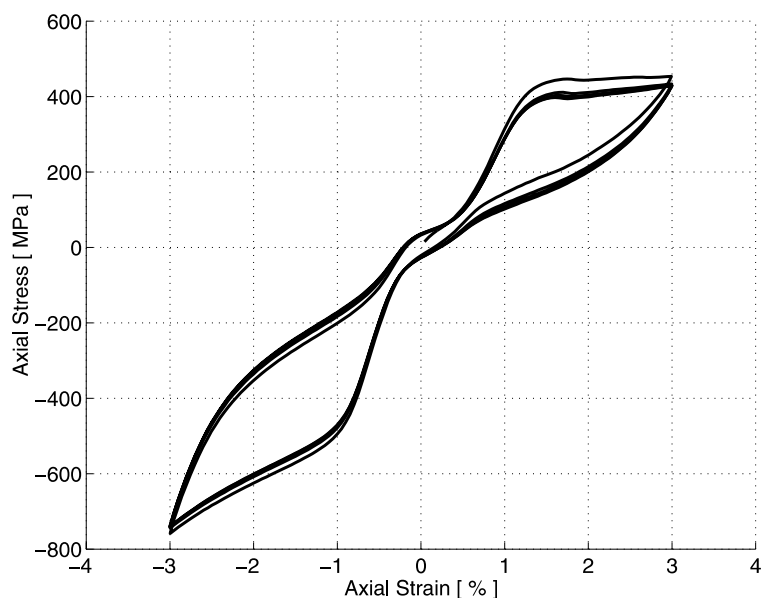
Fig. 1. An example of typical superelastic response in tension and compression: stress–strain response. The experimental data are taken from the work of Lim and McDowell (1999).

This unique macroscopic behavior has attracted an increasing scientific and commercial interest since it can be exploited in innovative applications (Duerig et al., 1990, Pelton et al., 1995, 1997), ranging from orthodontic wires for the correction of tooth malpositions (orthodontic appliances) to micro-structures used in the treatment of blood-vessel occlusions (stents).

As usual, the macroscopic response finds its justification looking at the underlying micro-level. In fact, shape-memory materials are able to undergo reversible martensitic transformations (Funakubo, 1987), that is, solid–solid, diffusionless transformations between a crystallographically more-ordered parent phase (*austenite*) and a crystallographically less-ordered product phase (*martensite*).

However, as addressed in several references (Chrysochoos et al., 1995, 1996; Lim and McDowell, 1999; Shaw and Kyriakides, 1995, 1997; Tobushi et al., 1998), experimental investigations on the macroscopic superelastic behaviour reveal that

- the response is often associated to significative temperature variations. Relying again on Lim and McDowell (1999), Fig. 2 shows the temperature–strain relation corresponding to the stress–strain curve of Fig. 1,
- the austenite–martensite phase transformations occur in well-defined stress–temperature ranges and they can be induced through mechanical loading–unloading patterns through thermal cooling–heating patterns or through combined mechanical–thermal patterns (Funakubo, 1987; Melton, 1990).

Recalling also that the typical superelastic stress–strain response is characterized by an hysteresis (Fig. 1), we may then conclude that SMAs show a strong thermo-mechanical constitutive coupling. This coupling is such that it possibly changes the material mechanical response during cyclic tests as a consequence of a progressive heating. This aspect can be of non-negligible importance in many applications; an example could be the use of superelastic materials as dissipative devices in the dynamics of structural elements, such as in the case of civil structures subject to earthquakes or in the case of light space structures under deployment conditions.
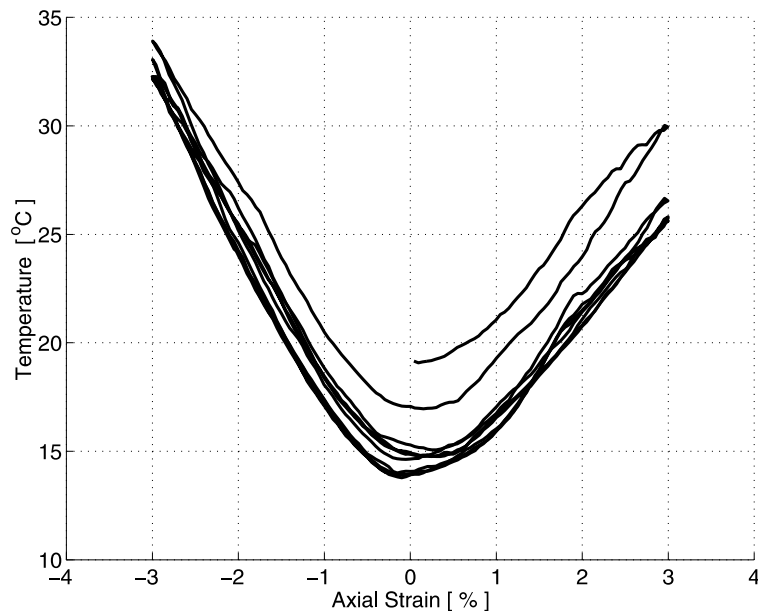
Fig. 2. An example of typical superelastic response in tension and compression: temperature–strain response. The experimental data are taken from the work of Lim and McDowell (1999).

Motivated by the described experimental observations in combination with modelling and applicative possible interests, several authors have studied the coupled thermo-mechanical problem of a superelastic shape-memory alloy wire. In the following, we briefly comment on some of the approaches available in the literature.

Leo et al. (1993) consider a temperature-dependent nonlinear thermoelastic model, including a heat generation mechanism at the austenite–martensite interface. Classifiable as a micro-level approach (due to the interface description), the work assumes a constant temperature for the wire cross-section, it considers that either one or two interfaces may occur in the wire and it limits the discussion only to the case of a monotonic loading.

Similarly, Bekker and Brinson (1997) deal again with a single austenite–martensite interface, while the model construction is based on a combination of phase diagram kinetics, macro-scale constitutive laws and energy balance considerations.

A different approach is pursued by Boyd and Lagoudas (1996a,b), who combine a micro- and macro-scale approach. In particular, the micro-scale description is very accurate, leading at the end to a complete but at the same time quite complex three-dimensional thermo-mechanical model.

Following a similar but simplified line of thinking, Shu et al. (1997) couple a one-dimensional SMA constitutive model with the thermal equations, considering the heat produced by electrical conduction in the wire. Again, the wire temperature is set to be constant within the cross-section, and hence, the whole thermo-mechanical problem is one-dimensional.

A similar 1D approach is proposed by Chrysochoos et al. (1995, 1996), where detailed experimental thermo-mechanical considerations are also addressed.

With respect to the cited literature, in the following, we approach the thermo-mechanical response of a superelastic SMA wire from a different perspective. In fact, our goal is the development of a computational framework for the simulation of SMA devices, made of beam elements with generic cross-sections and undergoing complex cyclic loadings. To do so, we start introducing the kinematical assumptions that plane

sections in the underformed configuration remain plane also in the deformed configuration and that the wire shear deformation is negligible.

Hence, choosing a macro-level description for the SMA response, we adopt a phenomenological one-dimensional stress–strain equation to describe the local mechanical behaviour. The model is cast within the general and flexible internal variable framework discussed by Lubliner and Auricchio (1996), and it properly describes the material different response in tension and compression. Moreover, it involves a scalar internal variable, representing the martensite fraction, variable for which evolutionary equations are proposed.

We also wish to emphasize that in the modeling, we are not describing any material interface, either because we assume to work with a representative average volume large enough to not require such a detailed micro-level description or because we assume to deal only with alloys for which the experimentally observed deformation is homogeneous from a macroscopic point of view.

The constitutive model is thermo-mechanically coupled due to the presence of internal heat sources in the form of phase-transition latent heat and mechanical dissipation. In particular, the transient coupled thermo-mechanical problem is approached considering the thermal evolution within the cross-section, hence as a two-dimensional problem.

We address a numerical scheme for the model time-integration and for the algorithmic solution of the corresponding time-discrete thermo-mechanical problem within a finite element method. The proposed framework makes it possible to study wires with a generic cross-section and subject to any cyclic stretching–bending loading condition.

Finally, results from numerical simulations are presented to show the response of a wire with circular cross section under cyclic stretching and cyclic bending loading conditions imposed at different strain rates.

2. Time-continuous model

We now address a one-dimensional thermo-mechanical time-continuous superelastic model, developed within the theory of irreversible thermodynamics (Lemaitre and Chaboche, 1990; Lubliner, 1990).

2.1. General framework

We assume that at each instant, the thermodynamic state of a homogenized volume element is characterized by an appropriate set of external (controllable) and internal variables. In particular, we choose as external variables the uniaxial strain, ε, and the absolute temperature, T, and as internal variable a scalar quantity, ξ_S, representing the martensite volume fraction.

A fundamental ingredient is then the free energy, ψ, function of the external and the internal variables. Based on the free energy, it is possible to derive consistent expressions for the dependent variables, such as the stress, σ and the entropy, η, defined as

$$\sigma = \frac{\partial \psi}{\partial \varepsilon}, \qquad \eta = \frac{\partial \psi}{\partial T}. \tag{1}$$

2.2. Strain decomposition

Limiting the discussion to a small deformation regime, we introduce the following additive decomposition:

$$\varepsilon = \varepsilon^{el} + \varepsilon^{in}, \tag{2}$$

where

- $\varepsilon^{\mathrm{el}}$ represents the thermo-elastic strain; by definition, it depends only on the control variables, i.e., $\varepsilon^{\mathrm{el}} = \varepsilon^{\mathrm{el}}(\sigma, T)$, and it includes contributions like the pure elastic term as well as the thermo-elastic expansion term.
- $\varepsilon^{\mathrm{in}}$ represents the inelastic strain, which may depend also on the set of internal variables, that is, in the present case on the martensite fraction ξ_{S}.

Generalizing a common statement within shape-memory literature (Auricchio et al., 1997; Auricchio and Taylor, 1997; Brinson, 1993; Brinson et al., 1996), we express the inelastic strain as

$$\varepsilon^{\mathrm{in}} = \varepsilon_L \xi_{\mathrm{S}} s \tag{3}$$

where

- ε_L is a measure of the maximum deformation obtainable aligning the martensite in one direction, often indicated as maximum residual strain (Funakubo, 1987) and in the following considered as a material parameter.
- s is the stress sign, that is,
$$\begin{aligned} s &= 1 \quad \text{if } \sigma > 0, \\ s &= -1 \quad \text{if } \sigma < 0. \end{aligned} \tag{4}$$

Hence, dealing only with uniaxial states of stress and assuming to distinguish between tensile and compressive material parameters with a+ or a− superscripts, Eq. (3) specializes to

$$\begin{aligned} \varepsilon^{\mathrm{in},+} &= \varepsilon_L^+ \xi_{\mathrm{S}} \quad \text{if } \sigma > 0, \\ \varepsilon^{\mathrm{in},-} &= -\varepsilon_L^- \xi_{\mathrm{S}} \quad \text{if } \sigma < 0. \end{aligned} \tag{5}$$

with ε_L^+ and ε_L^- both positive quantities.

At this point, we wish to highlight that for a one-dimensional case, it is important to distinguish between tensile and compressive material properties since experimental investigations have clearly evidenced a significative asymmetry between tension and compression (Gall et al., 1999; Huang, 1999; Liu et al., 1998; Manach and Favier, 1991; Orgéas and Favier, 1991).

However, in the forthcoming discussion, for brevity, we omit the superscripts + and − from the material constants when no confusion can be induced.

2.3. Free energy

After a critical review of the several proposals available in the literature (see also developments and comments in Appendix A) and adopting the subscripts A and S to indicate material parameters relative to the austenite and to the martensite, respectively, we assume the following free energy:

$$\begin{aligned} \psi &= [(u_{\mathrm{A}} - T\eta_{\mathrm{A}}) - \xi_{\mathrm{S}}(\Delta u - T\Delta\eta)] + C\left[(T - T_0) - T\log\frac{T}{T_0}\right] + \tfrac{1}{2}E(\varepsilon - \varepsilon_L\xi_{\mathrm{S}} s)^2 \\ &\quad - (T - T_0)(\varepsilon - \varepsilon_L\xi_{\mathrm{S}} s)E\alpha, \end{aligned} \tag{6}$$

where

- u_{A} and η_{A} are the internal energy and the entropy of the austenite.
- Δu and $\Delta\eta$ are the internal energy difference and the entropy difference between the austenite and the martensite. In particular, we set
$$\begin{aligned} \Delta u &= u_{\mathrm{A}} - u_{\mathrm{S}} \geqslant 0, \\ \Delta\eta &= \eta_{\mathrm{A}} - \eta_{\mathrm{S}} \geqslant 0 \end{aligned}$$

with u_S and η_S, the internal energy and the entropy of the martensite.
- C is the material heat capacity.
- T_0 is the natural or reference state temperature.
- E is the elastic modulus.
- α is the thermal expansion factor.

According to Eq. (1), the stress σ and the entropy η are

$$\sigma = \frac{\partial \psi}{\partial \varepsilon^{\mathrm{el}}} = \frac{\partial \psi}{\partial \varepsilon} = E(\varepsilon - \varepsilon_L \xi_S \ s) - E\alpha(T - T_0), \tag{7}$$

$$\eta = -\frac{\partial \psi}{\partial T} = \eta_A - \xi_S \Delta \eta + C \log \frac{T}{T_0} + (\varepsilon - \varepsilon_L \xi_S \ s)E\alpha. \tag{8}$$

2.4. Heat equation

Following classical textbooks (Lemaitre and Chaboche, 1990), the heat equation can be written as

$$C\dot{T} + \operatorname{div}\boldsymbol{q} = b, \tag{9}$$

where div indicates the divergence operator, a superposed dot indicates a time-derivative and $\boldsymbol{q}$ is the heat flux. In particular, under the validity of the Fourier law, we have $\boldsymbol{q} = -K\operatorname{grad} T$ with K, the thermal conductivity. Finally, b is the heat source, which can be written as

$$b = \mathscr{H}_{\mathrm{tmc}} + \mathscr{D}_{\mathrm{mec}}, \tag{10}$$

where

- $\mathscr{H}_{\mathrm{tmc}}$ represents the heat production associated to the thermo-mechanical coupling (including thermo-elastic effects, the phase transformation latent heat, etc.) and it is defined as

$$\mathscr{H}_{\mathrm{tmc}} = T \frac{\partial^2 \psi}{\partial T \partial \varepsilon} \dot{\varepsilon} + T \frac{\partial^2 \psi}{\partial T \partial \xi_S} \dot{\xi}_S. \tag{11}$$

- $\mathscr{D}_{\mathrm{mec}}$, briefly indicated as mechanical dissipation, represents the heat production associated to the dissipative mechanical processes and it is defined as

$$\mathscr{D}_{\mathrm{mec}} = \sigma\dot{\varepsilon} - \left(\frac{\partial \psi}{\partial \varepsilon} \dot{\varepsilon} + \frac{\partial \psi}{\partial \xi_S} \dot{\xi}_S \right). \tag{12}$$

We recall that the mechanical dissipation is in general required to be non-negative, i.e., $\mathscr{D}_{\mathrm{mec}} \geqslant 0$.

Due to the specific form of free energy chosen, we have

$$\mathscr{H}_{\mathrm{tmc}} = T\left[-E\alpha\dot{\varepsilon} + (\varepsilon_L E\alpha + \Delta\eta)\dot{\xi}_S \right], \tag{13}$$

$$\mathscr{D}_{\mathrm{mec}} = \Pi_1 \dot{\xi}_S \tag{14}$$

with

$$\Pi_1 = \varepsilon_L|\sigma| - T\Delta\eta + \Delta u \tag{15}$$

representing the thermodynamic force associated to ξ_S.

Finally, we note that the mechanical strain rate $\dot{\varepsilon}$ in Eq. (13) is a known quantity. In fact, as addressed in Section 1, at each instant t, we assume to know the history of the cross-section kinematical parameters,

which are the central axis elongation and the curvature, indicated as $\varepsilon_0 = \varepsilon_0(t)$ and $\chi = \chi(t)$, respectively. The strain, ε and the strain rate, $\dot{\varepsilon}$ in the generic fiber of the cross-section are then computed as

$$
\begin{aligned}
\varepsilon &= \varepsilon_0 + y\chi, \\
\dot{\varepsilon} &= \dot{\varepsilon}_0 + y\dot{\chi},
\end{aligned}
\tag{16}
$$

where y is the fiber offset.

2.5. Internal variable evolution

We assume to work with two processes which may produce variations of the martensite fraction:

- the conversion of austenite into martensite (A → S),
- the conversion of martensite into austenite (S → A).

For each process, the martensite evolution is expressed in terms of the associated driving force Π_1 derived in Eq. (15). It is interesting to observe that without losing any information, the driving force can be expressed as

$$
F = |\sigma| - TA,
\tag{17}
$$

where

$$
A = \frac{\Delta\eta}{\varepsilon_L}.
\tag{18}
$$

Eq. (17) is consistent with experimental evidences (Funakubo, 1987; Melton, 1990), showing that both processes are driven by either stress and/or temperature and that they may occur in stress-temperature regions delimited with good approximations by straight lines.

Following Likhachev and Koval (1992) as well as other references (Auricchio et al., 1997; Auricchio and Taylor, 1997; Auricchio and Sacco, 1999), we choose linear kinetic rules:

$$
\dot{\xi}_\mathrm{S} = -\mathscr{H}^{\mathrm{AS}}(1 - \xi_\mathrm{S})\frac{\dot{F}}{F - R_\mathrm{f}^{\mathrm{AS}}},
\tag{19}
$$

$$
\dot{\xi}_\mathrm{S} = \mathscr{H}^{\mathrm{SA}}\xi_\mathrm{S}\frac{\dot{F}}{F - R_\mathrm{f}^{\mathrm{SA}}}.
\tag{20}
$$

The terms $\mathscr{H}^{\mathrm{AS}}$ and $\mathscr{H}^{\mathrm{SA}}$ are activation factors relative to the two evolutionary processes, defined as

$$
\mathscr{H}^{\mathrm{AS}} = \begin{cases} 1 & \text{if } \begin{cases} R_s^{\mathrm{AS}} < F < R_\mathrm{f}^{\mathrm{AS}} \\ \dot{F} > 0 \end{cases}, \\ 0 & \text{otherwise} \end{cases}
\tag{21}
$$

$$
\mathscr{H}^{\mathrm{SA}} = \begin{cases} 1 & \text{if } \begin{cases} R_\mathrm{f}^{\mathrm{SA}} < F < R_s^{\mathrm{SA}} \\ \dot{F} < 0 \end{cases}, \\ 0 & \text{otherwise} \end{cases}
\tag{22}
$$

where

$$
\begin{aligned}
R_s^{\mathrm{AS}} &= \sigma_s^{\mathrm{AS}} - T_R A, & R_\mathrm{f}^{\mathrm{AS}} &= \sigma_\mathrm{f}^{\mathrm{AS}} - T_R A, \\
R_s^{\mathrm{SA}} &= \sigma_s^{\mathrm{SA}} - T_R A, & R_\mathrm{f}^{\mathrm{SA}} &= \sigma_\mathrm{f}^{\mathrm{SA}} - T_R A.
\end{aligned}
\tag{23}
$$

The quantities σ_s^{AS}, $\sigma_\mathrm{f}^{\mathrm{AS}}$, σ_s^{SA}, $\sigma_\mathrm{f}^{\mathrm{SA}}$ are material parameters indicating respectively the initial and final stress values for the A → S and the S → A transformations at temperature T_R. All these parameters can be

determined experimentally performing a uniaxial test inducing complete phase transformations at a temperature T_R, which is set only on the base of experimental convenience.

To guarantee the non-negativeness of the mechanical dissipation $\mathscr{D}_{\text{mec}}$, the material parameters σ_s^{AS}, σ_f^{AS}, σ_s^{SA}, σ_f^{SA} should verify the following inequalities:

$$\sigma_R \leqslant \sigma_s^{\text{AS}} \leqslant \sigma_f^{\text{AS}},$$
$$\sigma_f^{\text{SA}} \leqslant \sigma_s^{\text{SA}} \leqslant \sigma_R, \tag{24}$$

where σ_R is computed from the condition $\Pi_1 = 0$ for $T = T_R$, hence

$$\sigma_R = \frac{T_R \Delta\eta - \Delta u}{\varepsilon_L}. \tag{25}$$

3. Time-discrete model and algorithmic solution

The time-discrete model is obtained integrating the time-continuous model over the time interval $[t_n, t]$ through a backward-Euler integration scheme as discussed in the following. [1]

3.1. Heat equation

Integration of Eq. (9) leads to

$$C \frac{T - T_n}{t - t_n} + \operatorname{div} \boldsymbol{q} - b_d = 0, \tag{26}$$

where $\boldsymbol{q} = -K \operatorname{grad} T$, and

$$b_d = \frac{1}{t - t_n}[\Pi_1 \lambda_{\text{S}} + T\Gamma_1] \tag{27}$$

with

$$\lambda_{\text{S}} = \xi_{\text{S}} - \xi_{\text{S},n}$$
$$\Pi_1 = \varepsilon_L |\sigma| - T\Delta\eta + \Delta u \tag{28}$$
$$\Gamma_1 = -E\alpha(\varepsilon - \varepsilon_n) + (\varepsilon_L E\alpha + \Delta\eta)\lambda_{\text{S}}$$

with ε and ε_n assumed to be known.

3.2. Internal variable evolution

The time-discrete phase-transition rules are obtained from Eqs. (19) and (20), writing them in residual form and clearing fractions:

$$\mathscr{R}^{\text{AS}} = \lambda_{\text{S}}(F - R_f^{\text{AS}}) + \mathscr{H}_d^{\text{AS}}(1 - \xi_{\text{S}})(F - F_n) = 0 \tag{29}$$

$$\mathscr{R}^{\text{SA}} = \lambda_{\text{S}}(F - R_f^{\text{SA}}) - \mathscr{H}_d^{\text{SA}}\xi_{\text{S}}(F - F_n) = 0 \tag{30}$$

The quantity λ_{S} can be computed requiring the satisfaction of the active evolutionary equation.

To improve the numerical robustness of the solution procedure, we introduce two modifications to the model, as described in the following:

---

[1] To minimize the appearance of subscripts, the subscript n indicates a quantity that is evaluated at time t_n, while no subscript indicates a quantity that is evaluated at time t, with $t_n < t$.

1. We scale the phase transition driving force with respect to a temperature upper limit value, indicated as T_U. Accordingly, the driving force is now expressed as

$$F = |\sigma| - (T - T_U)A, \tag{31}$$

where the temperature T_U is an arbitrary temperature value such that $T < T_U$. With position 31, we guarantee the constant sign of F.

2. We convert the activation factors to a strain control approach, following the consideration of Auricchio and Sacco (1999). In particular, the time-discrete activation factors are defined as

$$\mathcal{H}_d^{AS} = \begin{cases} 1 & \text{if } \begin{cases} \hat{S}_s^{AS} < G < \hat{S}_f^{AS}, \\ G - G_n > 0, \end{cases} \\ 0 & \text{otherwise}, \end{cases} \tag{32}$$

$$\mathcal{H}_d^{SA} = \begin{cases} 1 & \text{if } \begin{cases} \hat{S}_f^{SA} < G < \hat{S}_s^{SA}, \\ G - G_n < 0, \end{cases} \\ 0 & \text{otherwise} \end{cases} \tag{33}$$

with

$$\begin{aligned}
G &= |\varepsilon| + \frac{A}{E}(T - T_U) \\
\hat{S}_s^{AS} &= \frac{\sigma_s^{AS}}{E} + \varepsilon_L \xi_{S,n}, \\
\hat{S}_f^{AS} &= \frac{\sigma_f^{AS}}{E} + \varepsilon_L, \\
\hat{S}_s^{SA} &= \frac{\sigma_s^{SA}}{E} + \varepsilon_L \xi_{S,n}, \\
\hat{S}_f^{SA} &= \frac{\sigma_f^{SA}}{E}.
\end{aligned} \tag{34}$$

3.3. Tangent modulus

We are now left only with the construction of the tangent modulus consistent with the time-discrete model. The use of a consistent tangent modulus preserves the quadratic convergence of the Newton method adopted for the solution of the heat equation.

Due to the specific problem under investigation (a wire under mechanical loading-unloadings), the strain ε is known at each instant and in each point of the cross-section. Hence, the thermal evolution within the cross-section is solved through a finite element method. Accordingly, we need to linearize the heat equation only with respect to the temperature. The only non-trivial term comes from the linearization of b_d (Eq. (27)):

$$db_d = \left(\frac{1}{t - t_n} \right)[d\Pi_1 \lambda_S + \Pi_1 d\lambda_S + d\Gamma_1 T + \Gamma_1 dT]. \tag{35}$$

Recalling Eq. (15), we have

$$d\Pi_1 = \varepsilon_L s\, d\sigma - \Delta\eta\, dT, \tag{36}$$

where

$$d\sigma = -E\varepsilon_L \, d\lambda_S - E\alpha \, dT. \tag{37}$$

So far, the only unknown left is $d\lambda_S$, which can be computed by linearizing the active discrete-time evolutionary equation, generally written as $\mathscr{R}(\lambda_S, T) = 0$. Accordingly,

$$d\mathscr{R} = \frac{\partial \mathscr{R}}{\partial \lambda_S} \, d\xi_S + \frac{\partial \mathscr{R}}{\partial T} \, dT = 0 \tag{38}$$

from which we obtain that

$$d\lambda_S = \left[-\left(\frac{\partial \mathscr{R}}{\partial \lambda_S} \right)^{-1} \frac{\partial \mathscr{R}}{\partial T} \right] dT. \tag{39}$$

4. Considerations on the model parameters

The described constitutive model is based on a specific set of material parameters. In particular, we have K, C, T_0, α, which are the thermal conductivity, the heat capacity, the initial (or natural) temperature and the thermal expansion factor, respectively. We also need to specify the elastic modulus as well as the internal energy and the entropy differences between the two phases, indicated respectively as E, Δu, $\Delta \eta$.

Moreover, chosen a convenient temperature T_R, we need to evaluate the stress values at which the two phase transitions (A $\rightarrow$ S and S $\rightarrow$ A) start and finish for $T = T_R$ under tension and compression as well as the corresponding residual strains. Indicated respectively as

$$\sigma_s^{AS,+}, \quad \sigma_f^{AS,+}, \quad \sigma_s^{SA,+}, \quad \sigma_f^{SA,+}, \quad \varepsilon_L^+,$$
$$\sigma_s^{AS,-}, \quad \sigma_f^{AS,-}, \quad \sigma_s^{SA,-}, \quad \sigma_f^{SA,-}, \quad \varepsilon_L^-,$$

these values can be experimentally determined performing a static (very slow) uniaxial tension–compression loading–unloading test.

However, in the forthcoming numerical examples, consistently with the thermodynamic approach adopted for the model development, we prefer to relate the material parameters relative to compression directly to the material parameters relative to tension. This is done assigning values to the parameters in tension and then assuming a value for the ratio, δ, defined as $\delta = A^+/A^-$; then, the compressive parameters can be computed as follows:

$$
\begin{aligned}
A^- &= A^+/\delta, & \varepsilon_L^- &= \Delta\eta/A^-, \\
\sigma_s^{AS,-} &= \delta\sigma_s^{AS,+}, & \sigma_f^{AS,-} &= \delta\sigma_f^{AS,+}, \\
\sigma_s^{SA,-} &= \delta\sigma_s^{SA,+}, & \sigma_f^{SA,-} &= \delta\sigma_f^{SA,+}.
\end{aligned}
\tag{40}
$$

5. Numerical examples

Using the time-discrete model addressed in Section 4, we now investigate the thermo-mechanical response of a superelastic wire under cyclic mechanical loadings. In particular, we focus on a circular cross-section wire with diameter $D = 2$ mm and, as discussed in Section 2.4, we assume to control the wire strain history through its elongation and curvature.

Due to symmetry considerations, only half cross-section is discretized using the mesh presented in Fig. 11.

To study the thermo-mechanical problem, we introduce 1D elements along the interface between the SMA wire and the external environment. These elements take into account the heat exchange between the

wire and the surrounding imposing that the flux is proportional through a material constant, V, to the difference of temperature between the wire and the surrounding.

Material parameters: The material parameters are

$K = 80 \text{ N s}^{-1} \text{ K}^{-1}$, $C = 4 \text{ N mm}^{-2} \text{ K}^{-1}$,

$T_0 = 293 \text{ K}$, $T_R = 573 \text{ K}$,

$E = 50\,000 \text{ MPa}$, $\alpha = 0 \text{ K}^{-1}$,

$\Delta u = 30 \text{ MPa}$, $\Delta \eta = 0.20 \text{ MPa K}^{-1}$,

$\sigma_s^{\text{AS},+} = 400 \text{ MPa}$, $\sigma_f^{\text{AS},+} = 500 \text{ MPa}$,

$\sigma_s^{\text{SA},+} = 300 \text{ MPa}$, $\sigma_f^{\text{SA},+} = 200 \text{ MPa}$,

$\varepsilon_L^+ = 7\%$, $\delta = 0.75$,

$V = 0.1$,

where T_0 indicates also the temperature of the surroundings. According to the value assigned to δ, we have:

$\sigma_s^{\text{AS},-} = 533 \text{ MPa}$, $\sigma_f^{\text{AS},-} = 666 \text{ MPa}$,

$\sigma_s^{\text{SA},-} = 400 \text{ MPa}$, $\sigma_f^{\text{SA},-} = 266 \text{ MPa}$,

$\varepsilon_L^- = 5.25\%$.

Loading histories: To investigate the thermo-mechanical response of the wire under different complex and cyclic loading conditions, we decide to assign the loading histories in terms of a non-dimensional time t_{adim}, always contained in the range $[0, 1]$; this choice helps in comparing results from different problems. The real time, t, is obtainable as follows:

$$t = (t_{\text{adim}} \times t_{\text{max}}) t_{\text{fact}} \tag{41}$$

that is, multiplying the non-dimensional time scale by the maximum non-dimensional time value t_{max} and then by a scaling factor, t_{fact}. In the following, for each single set of problems, t_{max} is fixed, while t_{fact} is varied; this corresponds to keep the same type of loading history and to change only the strain-rate at which it is applied.

Output quantities: Due to the loading situations under considerations, as mechanical outputs we consider the cross-section resulting force, F and resulting moment, M, defined respectively as:

$$F = \int_S \sigma \, \mathrm{d}S, \tag{42}$$

$$M = \int_S (y\sigma) \, \mathrm{d}S, \tag{43}$$

where S is the cross-section area. Moreover, due to the bi-dimensional nature of the problem and complexity of the solution, associated also with its evolutionary nature, as outputs, we also consider averaged values for the temperature and for the martensite fraction:

$$T_{\text{aver}} = \frac{1}{S} \int_S T \, \mathrm{d}S, \tag{44}$$

$$\xi_{\text{S,aver}} = \frac{1}{S} \int_S \xi_S \, \mathrm{d}S. \tag{45}$$

We also compute a measure of the spatial variance within the cross-section for both the wire temperature and the martensite fraction, defined respectively as the difference at each instant between the maximum and the minimum temperature and as difference at each instant between the maximum and the minimum martensite fraction in the wire cross-section:

$$T_{\text{var}} = T_{\text{max}} - T_{\text{min}}, \tag{46}$$

$$\xi_{S,var} = \xi_{S,max} - \xi_{S,min}. \tag{47}$$

Finally, we remark that all the material constants and computations relative to temperature are in term of Kelvin degrees; however, all the plots are in terms of Celsius degrees scaled with respect to the surrounding temperature (T_0).

5.1. Single-cycle uniaxial tension–compression test

We start the numerical investigations simulating a uniaxial tension–compression test. The loading history is presented in Table 1 (Load 1) in terms of the uniaxial elongation ε_0 versus the non-dimensional time t_{adim}, while the imposed curvature is kept identically equal to zero.

For the particular problem under investigation, we consider a t_{max} value equal to 24 s and scaling factors t_{fact} equal to $10^2, 1, 10^{-2}$ to which we will refer as the slow (S), medium (M) and fast (F) loading-rate case.

Fig. 3 reports the resulting force, F versus the applied elongation, ε_0 for the three cases. Similarly, Fig. 4 reports the average temperature T_{aver} with respect to the reference temperature, T_0.

It is interesting to observe that

- for the slow loading-rate case, the wire average temperature, T_{aver}, is constant and equal to the external temperature, T_0. Accordingly, the force–elongation response corresponds to the static case (no thermal transient),
- for the medium loading-rate case, the wire average temperature, T_{aver} oscillates around the external temperature T_0. Accordingly, the force–elongation response is partially above and partially below the static response. As a consequence, we may also note an increment of the hysteresis loop size,

Table 1
Loading histories in terms of non-dimensional time

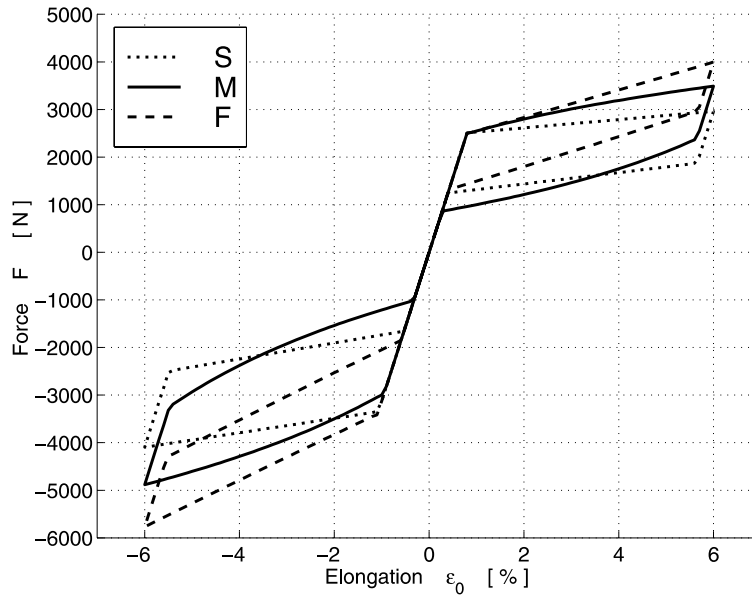|							
Load 1							
t_{adim} (–)	0	0.25	0.75	1			
ε_0 (–)	0	0.0600	−0.0600	0			
Load 2							
t_{adim} (–)	0	0.0286	0.0476	0.0667	0.0857	0.1048	0.1238
ε_0 (–)	0	0.0600	0.0200	0.0600	0.0200	0.0600	0.0200
	0.1429	0.1619	0.1810	0.2000	0.2190	0.2381	0.2714
	0.0600	0.0200	0.0600	0.0200	0.0600	0.0200	0.0900
	0.3095	0.3476	0.3857	0.4238	0.4619	0.5000	0.5381
	0.0100	0.0900	0.0100	0.0900	0.0100	0.0900	0.0100
	0.5762	0.6143	0.6524	0.6905	0.7286	0.7667	0.8524
	0.0900	0.0100	0.0900	0.0100	0.0900	0.0100	0.0900
	0.9476	1.0000					
	0	0					
Load 3							
t_{adim} (–)	0	0.0833	0.1333	0.1833	0.2333	0.2833	0.3333
χ (mm^{-1})	0	0.0500	0.0200	0.0500	0.0200	0.0500	0.0200
	0.3833	0.4333	0.4833	0.5333	0.5667	0.6000	0.6333
	0.0500	0.0200	0.0500	0.0200	0.0400	0.0200	0.0400
	0.6667	0.7000	0.7333	0.7667	0.8000	0.8333	0.9000
	0.0200	0.0400	0.0200	0.0400	0.0200	0.0400	0
	1.0000						
	0						

Fig. 3. Single-cycle uniaxial tension–compression test. Force, F versus elongation, ε_0 for different loading rates (S: slow; M: medium; F: fast).
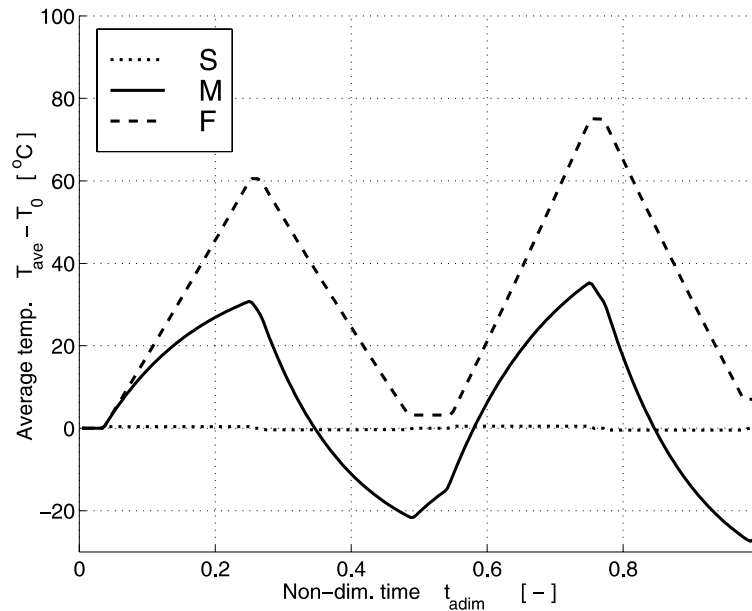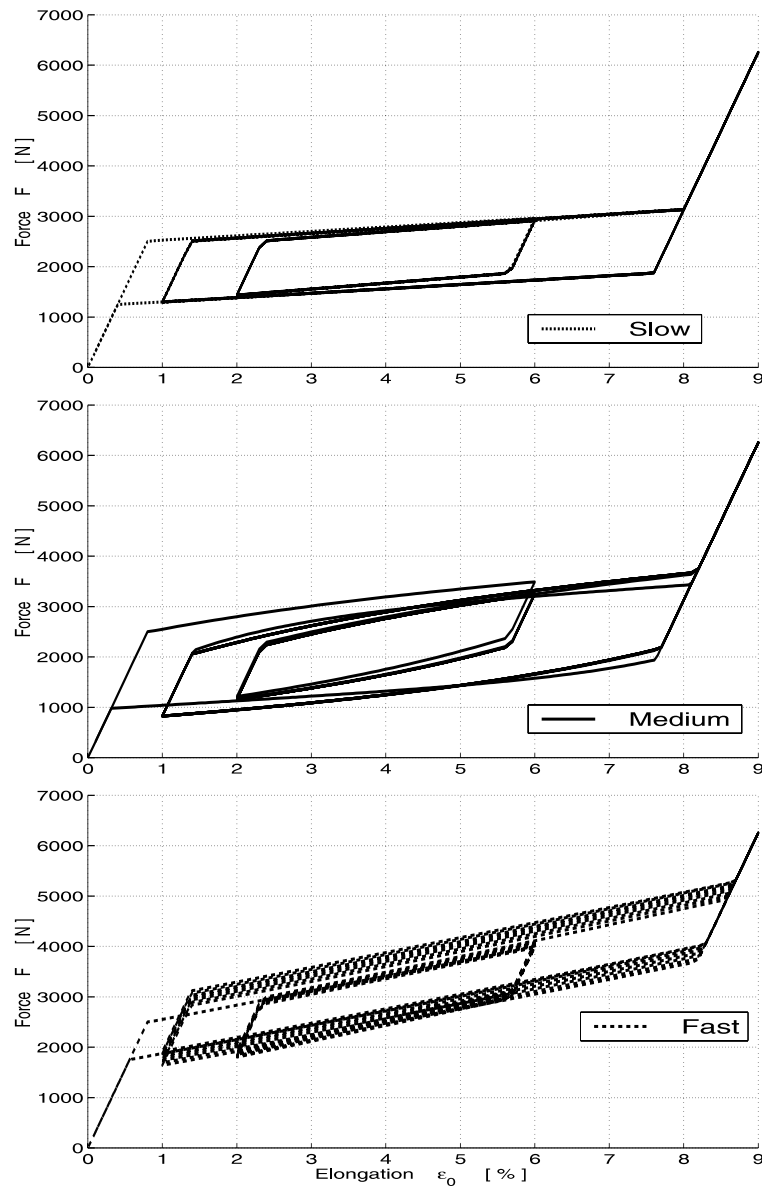
Fig. 4. Single-cycle uniaxial tension–compression test. Average temperature minus reference temperature, $T_{\mathrm{aver}} - T_0$ versus elongation, ε_0 for different loading rates (S: slow; M: medium; F: fast).

- for the fast loading-rate case, the wire average temperature, T_{aver}, oscillates above the external temperature T_0. Accordingly, the force–elongation response is always above the static response. As a consequence, we may also note a decrement of the hysteresis loop size.

For the present problem, the variances relative to the wire temperature and to the martensite fraction as defined in Eqs. (46) and (47) are computed but not reported since they show variations less than 1%.

5.2. Multiple-cycle uniaxial tension test

We now simulate a cyclic uniaxial tension test. The loading history is presented in Table 1 (Load 2) in terms of the uniaxial elongation ε_0 versus the non-dimensional time t_{adim}, while the imposed curvature is kept identically equal to zero.

Fig. 5. Multiple-cycle uniaxial tension test. Force, F versus elongation, ε_0 for different loading rates.

For the particular problem under investigation, we consider a t_{max} value equal to 210 s and scaling factors t_{fact} equal to $10^2, 1, 10^{-2}$ to which we will refer as slow (S), medium (M) and fast (F) loading-rate case.

Fig. 5 reports the resulting force, F, versus the applied elongation, ε_0, for the three cases. Similarly, Fig. 6 reports the average temperature, T_{aver}, with respect to the reference temperature, T_0.

It is interesting to observe that

- for the slow loading-rate case, the wire average temperature, T_{aver}, is constant and equal to the external temperature, T_0. Accordingly, the force–elongation response corresponds to the static case (no thermal transient),
- for the medium loading-rate case, the wire average temperature, T_{aver}, keeps oscillating around the external temperature, T_0. Accordingly, the force–elongation response is partially above and partially below the static response. As a consequence, we may also note an increment of the hysteresis loop size,
- for the fast loading-rate case, the wire average temperature, T_{aver}, oscillates above the external temperature T_0 and it progressively keeps increasing. Accordingly, the force–elongation response is always above the static response and it is possible to note a progressive decrement of the hysteresis loop size.

During each instant of the solution process, we also compute the variances T_{var} and $\xi_{S,var}$. However, also for this problem, the two variances are not reported since they show variations in the variables less than 1%.

5.3. Multiple-cycle bending test

We now simulate a cyclic bending test. The loading history is presented in Table 1 (Load 3) in terms of curvature χ versus non-dimensional time t_{adim}, while the axial elongation is kept identically equal to zero.
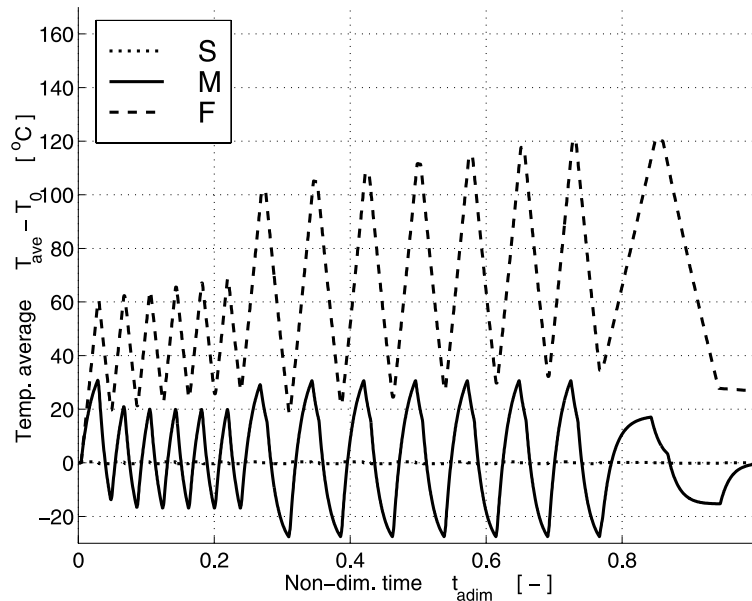

Fig. 6. Multiple-cycle uniaxial tension test. Average temperature minus reference temperature, $T_{aver} - T_0$ versus non-dimensional time, t_{adim} for different loading rates (S: slow; M: medium; F: fast).
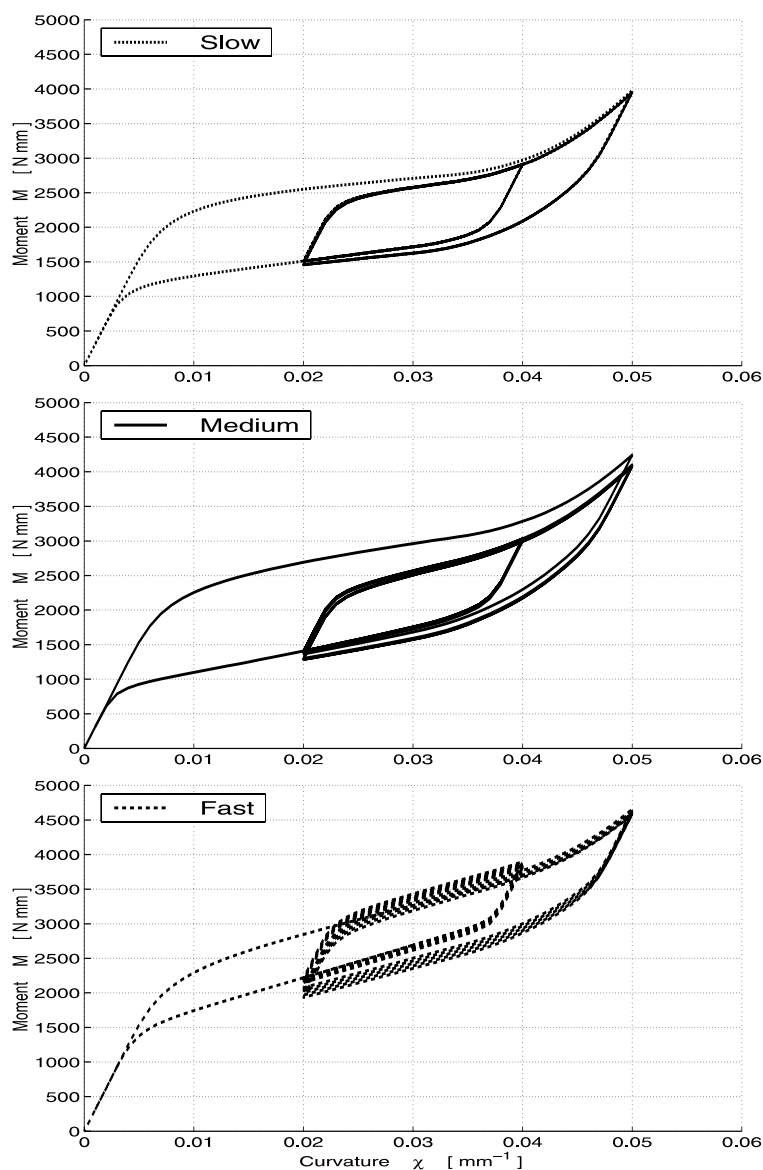
Fig. 7. Multiple-cycle bending test. Moment, M versus curvature, χ for different loading rates.

For the particular problem under investigation, we consider a t_{max} value equal to 60 s and scaling factors t_{fact} equal to 10^2, 1, 10^{-4} to which we will refer as slow (S), medium (M) and fast (F) loading-rate case.

Figs. 7–8 report the resulting moment, M and force, F, versus the applied curvature, χ, for the three cases. Similarly, Figs. 9 and 10 report the temperature average value, T_{aver}, and the temperature variance $\xi_{S,aver}$, respectively.

It is interesting to observe that

• for all the loading-rate cases, a non-zero resulting force is necessary to kept the elongation equal to zero. This can be easily explained recalling the different material response in tension and compression,
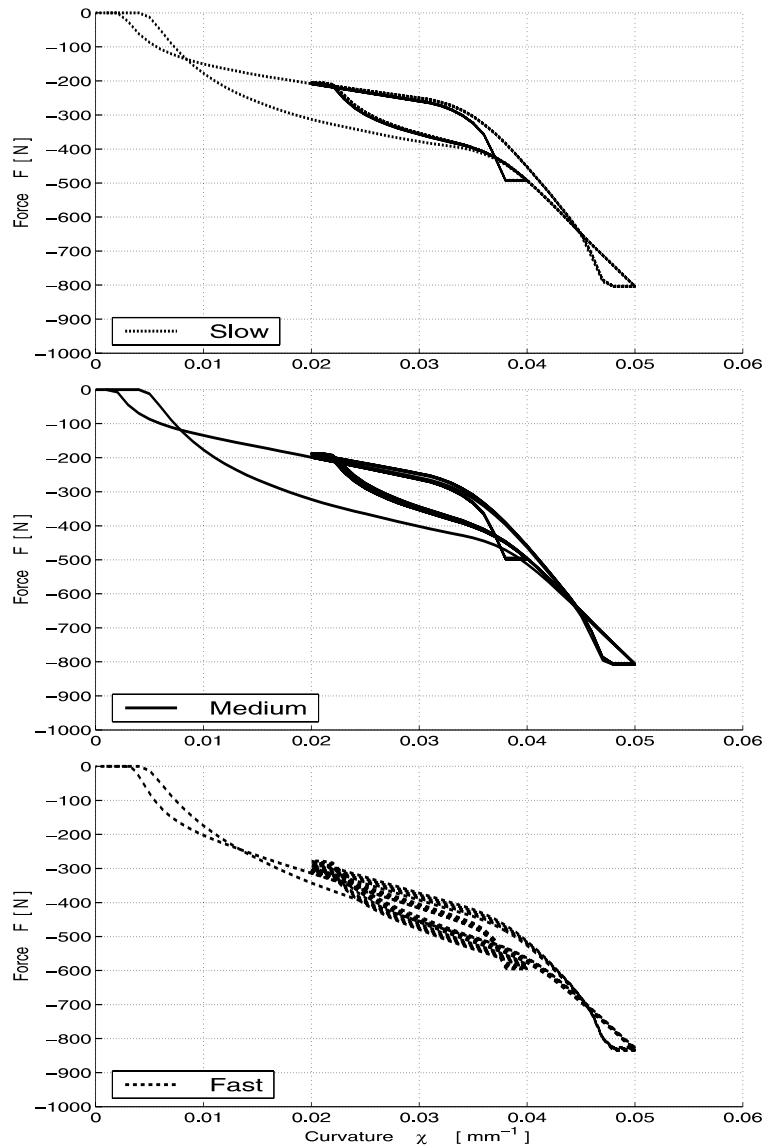
Fig. 8. Multiple-cycle bending test. Force, F versus curvature, χ for different loading rates.

- for the slow loading-rate case, the wire average temperature, T_{aver} is almost constant and equal to the external temperature, T_0. Accordingly, the moment–curvature response is very close to the static case (no thermal transient),
- for the medium loading-rate case, the wire average temperature, T_{aver}, keeps oscillating around the external temperature, T_0. Accordingly, the moment–curvature response is partially above and partially below the static response. As a consequence, we may also note an increment of the hysteresis loop size,
- for the fast loading-rate case, the wire average temperature, T_{aver}, oscillates above the external temperature, T_0 and it progressively keeps increasing. Accordingly, the moment–curvature response is always above the static response, and it is possible to note a progressive decrement of the hysteresis loop size.
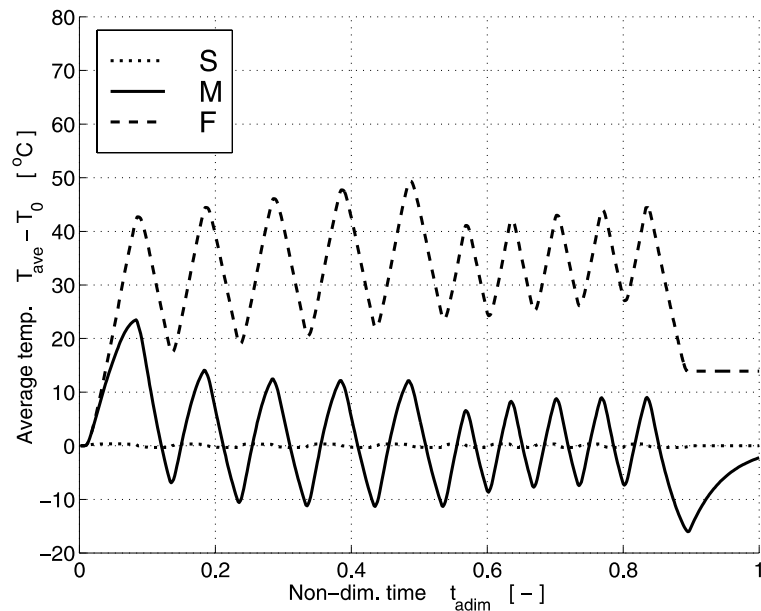
Fig. 9. Multiple-cycle bending test. Average temperature minus reference temperature, $T_{\text{aver}} - T_0$ versus adimensional time, t_{adim} for different loading rates (S: slow; M: medium; F: fast).
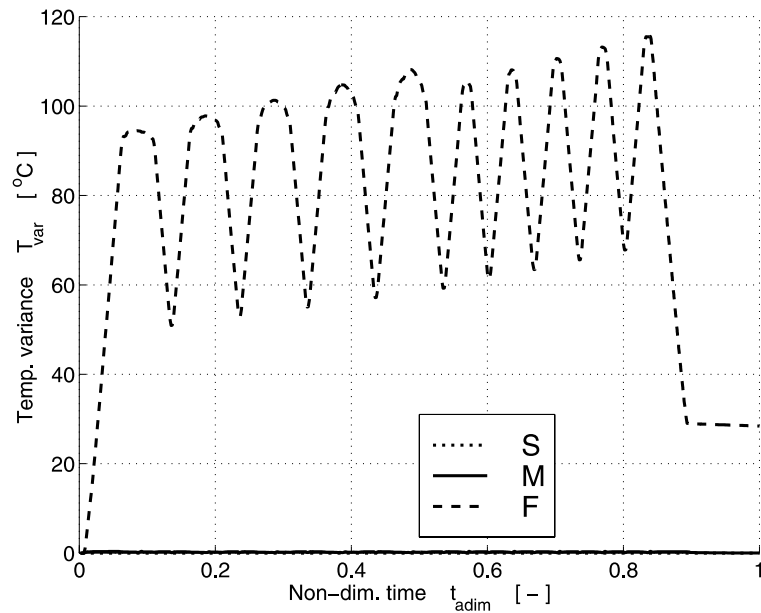

Fig. 10. Multiple-cycle bending test. Temperature variance, T_{var} versus non-dimensional time, t_{adim} for different loading rates (S: slow; M: medium; F: fast).

During each instant of the solution process, we also compute the martensite fraction average value, $\xi_{\text{S,aver}}$, and the martensite variance value, $\xi_{\text{S,var}}$. However, also for this problem, they are not reported since
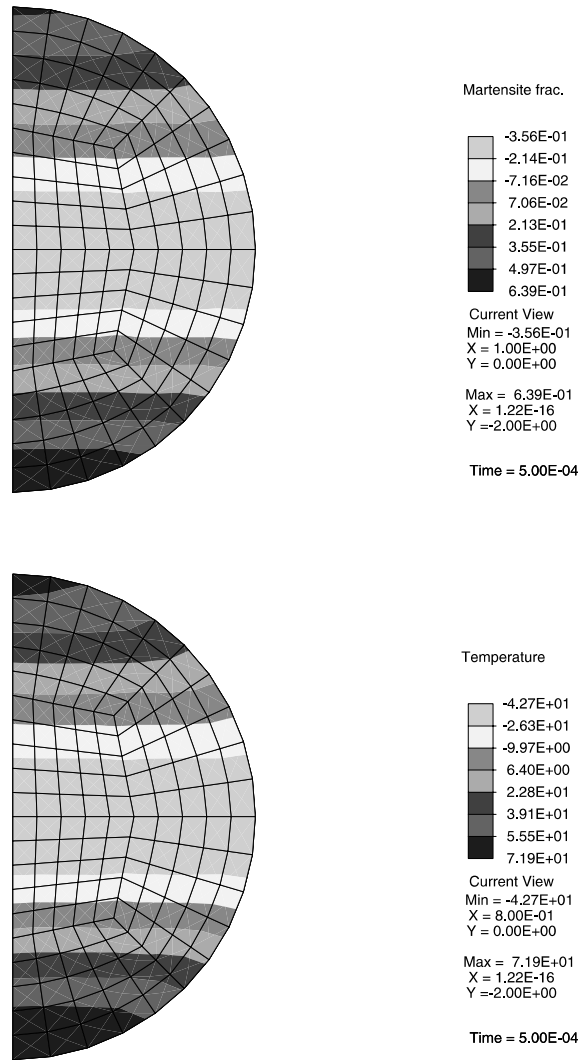
Fig. 11. Multiple-cycle bending test. Distribution within the cross-section of the quantities: $\xi_S - \xi_{S,aver}$ (i.e., martensite fraction minus martensite fraction average) and $T - T_{aver}$ (that is, temperature minus temperature average).

they show variation almost non-appreciable variations. However, to give an idea of the variability of the temperature and of the martensite fraction within the cross-section, Fig. 11 reports the quantities, $T - T_{aver}$ and $\xi_S - \xi_{S,aver}$ within the cross-section.

6. Conclusions

Comparing the available experimental data (Chrysochoos et al., 1996; Lim and McDowell, 1999) with the numerical results, we may conclude that, through the inclusion of the thermo-mechanical coupling in the modelling, it is possible to reproduce most of the effects observed experimentally in SMA when tested at different loading rates. In general, the numerical examples presented proved

- the strong coupling between the mechanical and the thermal material response,
- the need to operate in specific loading-rate ranges if the size of the hysteresis loop has to be maximized.

These considerations highlight the importance of thermo-mechanical analyses for SMA and the need for more accurate experimental investigations in order to better understand the nature of the macroscopic rate-dependent phenomena occurring in this class of materials.

Acknowledgements

Appendix A. A plausible free energy for a shape-memory alloy

Over the years, researchers have proposed many different free-energy expressions for materials undergoing martensitic phase transformations and in particular for shape-memory alloys. Examples – and clearly by no means exhaustive of the literature richness on the subject – can be found in references (Abeyaratne and Knowles, 1993; Boyd and Lagoudas, 1994, 1996a; Goo and Lexcellent, 1997; Huang and Brinson, 1998; Huo and Müller, 1993; Leclercq and Lexcellent, 1996; Levitas, 1994; Lu and Weng, 1997, 1998; Müller and Xu, 1991; Patoor et al., 1988; Raniecki et al., 1992; Song et al., 1991; Sun and Hwang, 1993a,b).

However, due to the possible confusion generated by all the different approaches, the appendix is devoted to a simple derivation of the form adopted in the present paper. In particular, we start considering the case of a single-phase material, then proposing a generalization to the case of a material undergoing solid–solid phase transformations.

A.1. Single-phase material

For a single-phase material, the free energy can be considered to be a function of the thermo-elastic strain, ε^{el} and of the temperature, T. Following Raniecki and Bruhns (1991), a possible form is

$$\psi = \psi(\varepsilon^{el}, T) = \psi_0(T) + \psi^{el}(\varepsilon^{el}) - (T - T_0)\eta^{el}(\varepsilon^{el}, T) + C\left[(T - T_0) - T \log\frac{T}{T_0}\right], \tag{A.1}$$

where

- ψ_0 is the material free energy in the natural or reference state, that is, for $T = T_0$ and $\varepsilon^{el} = 0$. Recalling a fundamental relation (Callen, 1985), we set $\psi_0 = u_0 - T\eta_0$, with u_0 and η_0 the material internal energy and entropy in the reference state.
- ψ^{el} is the free energy increase due to the elastic strain for $T = T_0$. Assuming a linear response in the elastic range, we set

$$\psi^{el} = \tfrac{1}{2}E\left(\varepsilon^{el}\right)^2 \tag{A.2}$$

with E, the elastic modulus.

- η^{el} is the entropy increase due to the elastic strain for $T = T_0$; in fact,

$$\eta = -\frac{\partial \psi}{\partial T} = \eta_0 + \eta^{\text{el}}(\varepsilon^{\text{el}}) + C \log \frac{T}{T_0}. \qquad (A.3)$$

Assuming again a linear response, we set

$$\eta^{\text{el}}(\varepsilon^{\text{el}}) = \varepsilon^{\text{el}} E \alpha \qquad (A.4)$$

with α the thermal expansion factor.
- C is the material heat capacity; in fact,

$$T \frac{\partial \eta}{\partial T} = C. \qquad (A.5)$$

Rewriting the free energy and collecting term, the final form is

$$\psi = u_0 - T\eta_0 + \frac{1}{2} E\left(\varepsilon^{\text{el}}\right)^2 - (T - T_0)\varepsilon^{\text{el}} E \alpha + C\left[(T - T_0) - T \log \frac{T}{T_0}\right]. \qquad (A.6)$$

A.2. Material undergoing phase transformations

We now need to properly generalize the free energy proposed in Eq. (A.6) to the case of a material undergoing a solid–solid phase transformation between austenite and martensite.

We start recalling that in the present context, the phase transformation is described through the scalar internal variable, ξ_S, representing the martensite fraction. Accordingly, the conditions $\xi_S = 0$ and $\xi_S = 1$ indicate that the material is composed only of austenite or martensite, respectively.

Hence, as first step, we generalize Eq. (A.6) such that a free energy similar to the one relative to a single-phase material is returned for the limiting cases $\xi_S = 0$ and $\xi_S = 1$. With this goal in mind, we concentrate on the term $\psi_0 = u_0 - T\eta_0$.

Adopting subscripts A and S to indicate material parameters relative to the austenite and to the martensite, we set

$$\psi_0 = [u_A - T\eta_A] - \xi_S[\Delta u - T\Delta\eta] + \xi_S(1 - \xi_S)[u_{\text{int}} - T\eta_{\text{int}}], \qquad (A.7)$$

where

- u_A and η_A are the internal energy and the entropy of the austenite.
- Δu and $\Delta\eta$ are the internal energy difference and the entropy difference between the austenite and the martensite. In particular, we set

$$\Delta u = u_A - u_S \geqslant 0,$$

$$\Delta\eta = \eta_A - \eta_S \geqslant 0$$

with u_S and η_S the internal energy and the entropy of the martensite.
- the term with factor $\xi_S(1 - \xi_S)$ is a classical interaction contribution since it is zero for $\xi_S = 0$ or $\xi_S = 1$ and it is non-zero only for intermediate values of ξ_S. Hence, it models the variations in free energy due to the presence of an austenite–martensite mixture.

Accordingly, we may conclude that a plausible free energy for a material undergoing a solid–solid phase transformation may have the following form:

$$\psi = [(u_{\mathrm{A}} - T\eta_{\mathrm{A}}) - \xi_{\mathrm{S}}(\Delta u - T\Delta\eta)] + C\left[(T - T_0) - T\log\frac{T}{T_0}\right] + \frac{1}{2}E(\varepsilon - \varepsilon_L\xi_{\mathrm{S}}s)^2$$
$$- (T - T_0)(\varepsilon - \varepsilon_L\xi_{\mathrm{S}}s)E\alpha, \tag{A.8}$$

where we used Eq. (3) relating the thermo-elastic strain to the total and the inelastic strain and where we neglect the interaction term. [2]

It is interesting to observe that in general the elastic modulus E, the thermal expansion factor α and the heat capacity C can be assumed to be function of the internal variable ξ_{S}, that is,

$$E = E(\xi_{\mathrm{S}}), \qquad \alpha = \alpha(\xi_{\mathrm{S}}), \qquad C = C(\xi_{\mathrm{S}}) \tag{A.9}$$

However, for simplicity, in the following, they are all assumed to be independent of ξ_{S}.

References

Abeyaratne, R., Knowles, J., 1993. A continuum model of thermoelastic solid capable of undergoing phase transitions. Journal of the Mechanics and Physics of Solids 41, 541–571.

Auricchio, F., Sacco, E., 1999. A temperature-driven beam for shape-memory alloys: constitutive modelling, finite-element implementation and numerical simulations. Computer Methods in Applied Mechanics and Engineering 174, 171–190.

Auricchio, F., Taylor, R., 1997. Shape-memory alloys: modelling and numerical simulations of the finite-strain superelastic behavior. Computer Methods in Applied Mechanics and Engineering 143, 175–194.

Auricchio, F., Taylor, R., Lubliner, J., 1997. Shape-memory alloys: macromodelling and numerical simulations of the superelastic behavior. Computer Methods in Applied Mechanics and Engineering 146, 281–312.

Bekker, A., Brinson, L., 1997. Temperature-induced phase transformation in a shape memory alloy: phase diagram based kinetic approach. Journal of the Mechanics and Physics of Solids 45, 949–988.

Boyd, J., Lagoudas, D., 1994. A thermodynamical constitutive model for the shape-memory effect due to transformation and reorientation. In: Varadan, V. (Ed.), Proceedings of the International Society for Optical Engineering, Vol. 2189, pp. 276–288.

Boyd, J., Lagoudas, D., 1996a. A thermodynamical constitutive model for shape-memory materials. Part I. The monolithic shape-memory alloy. International Journal of Plasticity 12, 805–842.

Boyd, J., Lagoudas, D., 1996b. A thermodynamical constitutive model for shape-memory materials. Part II. The SMA composite materials. International Journal of Plasticity 12, 843–873.

Brinson, L., 1993. One-dimensional constitutive behavior of shape memory alloys: Thermomechanical derivation with non-constant material functions and redefined martensite internal variables. Journal of Intelligent Material Systems and Structures 4, 229–242.

Brinson, L., Bekker, A., Hwang, S., 1996. Deformation of shape memory alloys due to thermo-induced transformations. Journal of Intelligent Material Systems and Structures 7, 97–107.

Buehler, W., Wiley, R., 1965. Nickel-based alloys. Technical report, Naval Ordinance Lab. US-Patent 3174851.

Callen, H., 1985. Thermodynamics and an Introduction to Thermostatics. Wiley, New York.

Chrysochoos, A., Lobel, M., Maisonneuve, O., 1995. Thermomechanical coupling of pseudoelastic behaviour of CuZnAl and NiTi alloys. Comptes Rendus de l'Academie des Sciences SerieII 320, 217–223.

Chrysochoos, A., Pham, H., Maissonneuve, O., 1996. Energy balance of thermoelastic martensite transformation under stress. Nuclear Engineering and Design 162, 1–12.

Duerig, T., Melton, K., Stökel, D., Wayman, C. (Eds.), 1990. Engineering Aspects of Shape Memory Alloys. Butterworth-Heinemann, London.

Funakubo, H., 1987. Shape Memory Alloys. Gordon and Breach Science Publishers, New York (translated from the Japanese by Kennedy, J.B.,).

Gall, K., Sehitoglu, H., Chumlyakov, Y., Kireeva, I., 1999. Tension–compression asymmetry of the stress–strain response in aged single crystal and polycristalline NiTi. Acta Materialia 47, 1203–1217.

Goo, B., Lexcellent, C., 1997. Micromechanics-based modeling of two-way memory effect of a single crystalline shape-memory alloy. Acta Materialia 45, 727–737.

Huang, M., Brinson, L., 1998. A multivariant model for single crystal shape memory alloy behavior. Journal of the Mechanics and Physics of Solids 46, 1379–1409.

---

[2] We recall the thermo-elastic nature of the martensitic phase transformations occurring in shape-memory materials.

Huang, W., 1999. Yield surfaces of shape memory alloys and their applications. Acta Materialia 47, 2769–2776.

Huo, Y., Müller, I., 1993. Nonequilibrium thermodynamics of pseudoelasticity. Continuum Mechanics and Thermodynamic 5, 163–204.

Leclercq, S., Lexcellent, C., 1996. A general macroscopic description of the thermomechanical behavior of shape memory alloys. Journal of Mechanics and Physics of Solids 44, 953–980.

Lemaitre, J., Chaboche, J., 1990. Mechanics of Solid Materials. Cambridge University Press Cambridge, MA.

Leo, P., Shield, T., Bruno, O., 1993. Transient heat transfer effects on the pseudoelastic behavior of shape-memory wires. Acta Metallurgica Materialia 41, 2477–2485.

Levitas, V., 1994. Thermomechanical description of pseudoelasticity – the threshold-type dissipative force with discrete memory. Mechanics Research Communications 21, 273–280.

Likhachev, A., Koval, Y., 1992. On the differential equation describing the hysteretic behavior of shape memory alloys. Scripta Metallurgica et Materialia 27, 223–227.

Lim, T., McDowell, D., 1999. Mechanical behavior of an Ni–Ti alloy under axial–torsional proportional and non-proportional loading. Journal of Engineering Materials and Technology 121, 9–18.

Liu, Y., Xie, Z., Humbeeck, J.V., Delay, L., 1998. Asymmetry of stress–strain curves under tension and compression for NiTi shape memory alloys. Acta Materialia 46, 4325–4338.

Lu, Z., Weng, G., 1997. Martensitic transformations and stress–strain relations of shape-memory alloys. Journal of the Mechanics and Physics of Solids 45, 1905–1928.

Lu, Z., Weng, G., 1998. A self-consistent model for the stress–strain behavior of shape memory alloy polycrystals. Acta Materialia 46, 5423–5433.

Lubliner, J., 1990. Plasticity Theory. Macmillan, New York.

Lubliner, J., Auricchio, F., 1996. Generalized plasticity and shape memory alloys. International Journal Solids and Structures 33, 991–1003.

Manach, P., Favier, D., 1991. Experimental study for the identification of a tensorial scheme for shape memory alloys. Journal de Physique IV 1, 415–420.

Melton, K., 1990. Ni–Ti based shape memory alloys. In: Duerig, T., Melton, K., Stökel, D., Wayman, C. (Eds.), Engineering Aspects of Shape Memory Alloys, pp. 21–35.

Müller, I., Xu, H., 1991. On the pseudo-elastic hysteresis. Acta Metallurgica et Materialia 39, 263–271.

Orgéas, L., Favier, D., 1991. Stress-induced martensitic transformation of NiTi alloy in isothermal shear, tension and compression. Acta Materialia 46, 5579–5591.

Patoor, E., Eberhardt, A., Berveiller, M., 1988. Thermomechanical behaviour of shape memory alloys. Archives of Mechanics 40, 755–794.

Pelton, A., Hodgson, D., Russel, S., Duerig, T. (Eds.), 1997. Proceedings of the Second International Conference on Shape Memory and Superelastic Technologies, Asilomar, CA.

Pelton, A., Hodgson, D., Duerig, T., (Eds.), 1995. Proceedings of the First International Conference on Shape Memory and Superelastic Technologies, Asilomar, CA.

Raniecki, B., Bruhns, O., 1991. Thermodynamic reference model for elasto-plastic solids undergoing phase transitions. Arch. Mech. 43, 343–376.

Raniecki, B., Lexcellent, C., Tanaka, K., 1992. Thermodynamic models of pseudoelastic behaviour of shape memory alloys. Arch. Mech. 44, 261–284.

Shaw, J., Kyriakides, S., 1995. Thermomechanical aspects of NiTi. Journal of the Mechanics and Physics of Solids 43, 1243–1281.

Shaw, J., Kyriakides, S., 1997. On the nucleation and propagation of phase transformation fronts in a NiTi alloy. Acta Materialia 45, 683–700.

Shu, S., Lagoudas, D., Hughes, D., Wen, J., 1997. Modeling of a flexible beam actuated by shape memory alloy wires. Smart Materials and Structures 6, 265–277.

Song, G., Sun, Q., Cherkaoui, M., 1991. Role of microstructure in the thermomechanical behavior of SMA composites. Journal of Engineering Materials and Technology 39, 507–524.

Sun, Q., Hwang, K., 1993a. Micromechanics modelling for the constitutive behavior of polycrystalline shape memory alloys I. Derivation of general relations. Journal of the Mechanics and Physics of Solids 41, 1–17.

Sun, Q., Hwang, K., 1993b. Micromechanics modelling for the constitutive behavior of polycrystalline shape memory alloys. II. Study of the individual phenomena. Journal of the Mechanics and Physics of Solids 41, 19–33.

Tobushi, H., Shimeno, Y., Hachisuka, T., Tanaka, K., 1998. Influence of strain-rate on superelastic properties of Ti–Ni shape memory alloy. Mechanics of Materials 30, 141–150.

Wayman, C., 1992. Shape memory and related phenomena. Progress in Material Science 36, 203–224.

Wayman, C., 1993. Shape memory alloys. MRS bulletin April, 49–56.

Wayman, C., Duerig, T., 1990. An introduction to martensite and shape memory. In: Duerig, T., Melton, K., Stökel, D., Wayman, C. (Eds.), Engineering Aspects of Shape Memory Alloys pp. 3–20.